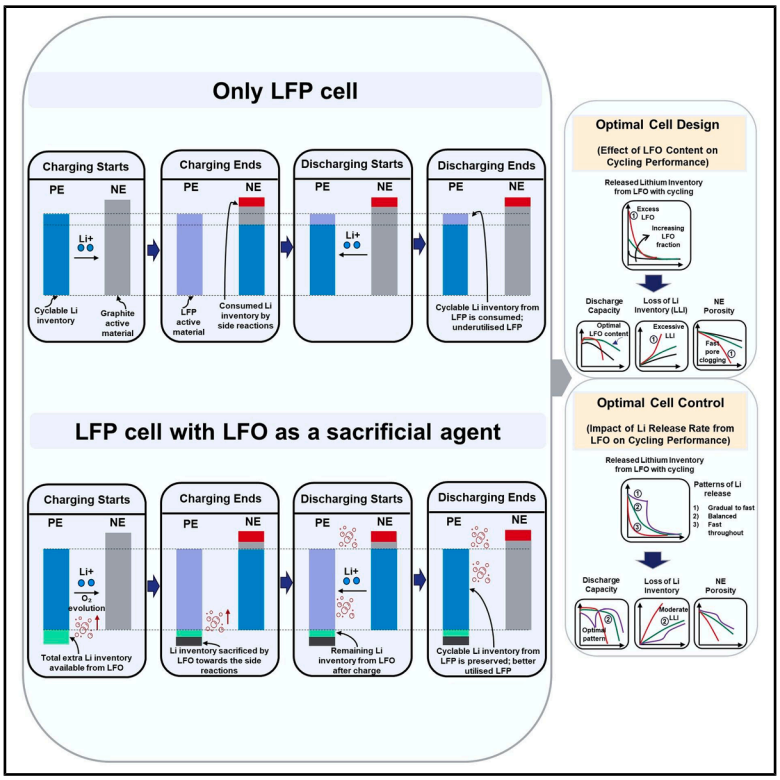
Cell Reports
Physical Science

Article

How to design a zero-degradation battery by compensating for loss of lithium inventory in LFP cells with LFO additives

Graphical abstract



Highlights

- "Zero degradation" requires controlled lithium release, optimal LFO, and good cell design
- Slow lithium release preserves cell balancing; fast release accelerates aging
- Optimal LFO content is a must; too little does not benefit, excess accelerates aging
- Anode oversizing (overhang) reduces degradation but lowers energy density

Authors

Sunil Kumar Rawat, Simon E.J. O'Kane, Ruihe Li, Gregory James Offer, Monica Marinescu

Correspondence

gregory.offer@imperial.ac.uk

In brief

Sunil et al., using the LFP-LFO composite cell model, show that "zero-degradation" batteries can be achieved by using lithium-rich additives such as LFO to compensate for lost lithium inventory, but only with careful control of lithium/oxygen release. Lithium release timing, optimum LFO amount, and suitable cell design changes are all critical.

Rawat et al., 2026, Cell Reports Physical Science 7, 103279
May 20, 2026 © 2026 The Authors. Published by Elsevier Inc.
https://doi.org/10.1016/j.xcrp.2026.103279

CellPress

Cell Reports
Physical Science

CellPress
OPEN ACCESS

Article

How to design a zero-degradation battery by compensating for loss of lithium inventory in LFP cells with LFO additives

Sunil Kumar Rawat,[1] Simon E.J. O'Kane,[1] Ruihe Li,[1] Gregory James Offer,[1,2,3,*] and Monica Marinescu[1,2]
[1]Department of Mechanical Engineering, Imperial College London, London SW7 2AZ, UK
[2]The Faraday Institution, Quad One, Becquerel Avenue, Harwell Campus, Didcot OX11 0RA, UK
[3]Lead contact
*Correspondence: gregory.offer@imperial.ac.uk
https://doi.org/10.1016/j.xcrp.2026.103279

SUMMARY

Loss of lithium inventory (LLI) remains the dominant degradation mode in lithium-ion cells, responsible for a reduced cycle life. Lithium-rich additives such as lithium iron oxide (Li_5FeO_4 [LFO]) have been proposed as sacrificial lithium sources to compensate for LLI. Recent reports from CATL and Rimac Energy claim "zero degradation" in commercial lithium iron phosphate (LFP)-LFO composite cells; however, the underlying mechanisms remain undisclosed and largely unexplored in the literature. Here, we report how LFO can be employed in commercial LFP cells using a full-cell physics-based model in PyBaMM to achieve the so-called "zero degradation." We design five controlled lithium release strategies to study the impact of lithium release speed (slow, fast) and timing (early, delayed/late in cell life) on cell degradation. We further identify the optimum LFO content in the LFP cathode to maximize cell life. The results show that slow, delayed/late lithium release maintains cell balancing and reduces degradation, whereas rapid, early release and excessive LFO accelerate aging. Additional anode overhang can mitigate this effect but introduces an energy density trade-off. Overall, achieving zero degradation requires optimal additive content, controlled/timed lithium release, and informed cell design.

INTRODUCTION

Loss of lithium inventory (LLI) is one of the major consequences of degradation and the reasons behind capacity fade and a reduced life cycle in lithium-ion batteries.[1,2] LLI is particularly intense during formation and the first few cycles of operation because of the initial formation of the solid electrolyte interphase (SEI). As the formation of SEI continues during cycling and calendar aging,[3–7] LLI continues to occur. Other degradation mechanisms, such as lithium plating,[8] also lead to the consumption of lithium ions and, hence, LLI. Recent breakthroughs in academic and industrial research have explored how LLI can be compensated by using an additive that can release additional lithium inventory, thus improving battery longevity.

Lithium iron oxide (LFO or Li_5FeO_4) is seen as an excellent lithium-rich additive due to its antifluorite structure that stores as much as four times (per gram) more lithium ions[9] compared to many conventional active materials, enabling it to achieve significantly higher theoretical and practical capacity per gram.[10,11] The lithium ions stored in the LFO are released irreversibly in two stages, at open circuit potentials (OCPs) vs. lithium of 3.5 and 4.0 V,[9,10] making it traditionally suitable only for primary cells. However, in a secondary cell, lithium release from the LFO has been demonstrated to compensate for LLI.[9–12] The use of LFO as a sacrificial agent in lab-scale coin cells showed that LFO can successfully compensate for LLI during cell formation and subsequent early charge-discharge cycles and help maintain stable cell performance. Companies such as CATL and Rimac Energy have demonstrated the commercial-scale viability of LFO being used in this way and claimed to have achieved zero apparent degradation.[13,14] CATL manufactured LFP cells with LFO as a cathode additive and reported zero apparent degradation for the first 1,000 cycles.[13] They hinted at operating the cell so that the release of lithium from LFO happens in the early phase of the cell's life. Rimac Energy reported to have operated the LFP-LFO composite cells using a slightly different approach. They focused on the gradual release of lithium from LFO to achieve zero capacity fade for two years.[14] Rimac Energy has also mentioned using an advanced power conversion system to achieve such performance. This highlights that, beyond the cell design, the control over operational conditions might be crucial to tap into the full potential of LFO additives. However, neither of the two companies has disclosed the exact methods, mechanisms, and strategies for successfully employing LFO as an additive in commercial cells, leaving researchers to speculate about the underlying principles. The commercial-level use of LFO and the underpinning scientific principles of how to use it are also missing in the peer-reviewed literature. Using these innovations as motivation, our work offers detailed insight into how LFO can be employed in commercial LFP cells with a composite

This is an open access article under the CC BY license (http://creativecommons.org/licenses/by/4.0/).

LFP-LFO positive electrode (PE) and graphite negative electrode (NE). To achieve this, we built a full-cell physics-based model framework in PyBaMM,[15] ran simulations, and analyzed the model predictions.

We first provide a detailed analysis of the underlying mechanisms of employing LFO in LFP cells through seven subsections in the results and discussion, covering (1) the mechanism of lithium and oxygen release from LFO in correlation with experimental half-cell OCP data for pure LFO; (2) the correlation of lithium and oxygen release to the full cell charging and discharging voltages in a single cycle; (3) lithium release from LFO during cell cycling; (4) the impact of released lithium from LFO on cell degradation, its capacity, and life; (5) detailed analysis of control methods for optimal lithium and oxygen release; (6) optimal LFO volume fraction to be used in LFP-LFO cells for achieving maximum cell performance; and (7) cell redesign approach to prevent cell unbalancing during an overlithiation scenario to achieve improved cell longevity. Thereafter, the methods present and discuss the model setup and its implementation, model assumptions, setting up virtual experiments, and methods for controlled lithium release from LFO in PyBaMM.

Our work significantly adds to the scientific understanding of the effect of LFO additives on the long-term performance and degradation of LFP-LFO composite cells and the behavior of so-called "zero-degradation" lithium-ion batteries. Using a full-cell physics-based model implemented in PyBaMM, we investigate the effects of releasing additional lithium from LFO on cell degradation, including SEI, lithium plating, porosity clogging, cell discharge capacity, and cell life. Different lithium release patterns are explored to compensate for lithium loss during cycling. Model predictions show that rapid lithium and oxygen release lead to intra-cell stoichiometric imbalances and increased degradation, whereas gradual release can maintain cell balancing, leading to longer cell life. We also show that an optimum LFO content exists; low amounts provide limited benefit, while excessive amounts accelerate degradation. Redesigning the cell to account for excess lithium release by oversizing NE capacity (overhang) improves long-term performance but introduces an energy density trade-off. These results show that achieving zero degradation requires careful optimization of LFO content, cell balancing, and lithium release strategies.

RESULTS AND DISCUSSION

Mechanism of lithium and oxygen release from LFO in correlation with its experimental OCP

LFO (Li_5FeO_4) material as a sacrificing agent in lithium-ion (Li^+) cells releases its lithium inventory as a result of the following two reactions:

$$Li_5FeO_4 \rightarrow Li_3FeO_{3.5} + 0.25O_2\uparrow + 2Li^+ + 2e^- \quad \text{(Equation 1)}$$

$$Li_3FeO_{3.5} \rightarrow LiFeO_2 + 0.75O_2\uparrow + 2Li^+ + 2e^-. \quad \text{(Equation 2)}$$

Two irreversible releases of Li^+ from LFO take place: one between LFO half-cell OCP of 3.5 and ~3.75 V (Equation 1) and the other between ~3.75 and 4.5 V (Equation 2).[10] Figure 1 shows the half-cell OCP of pure LFO material[10] vs. stoichiometry, exhibiting the two plateaus that correspond to the two stages of lithium release. Overall, each mole of LFO releases 4 moles of lithium across the full OCP range.

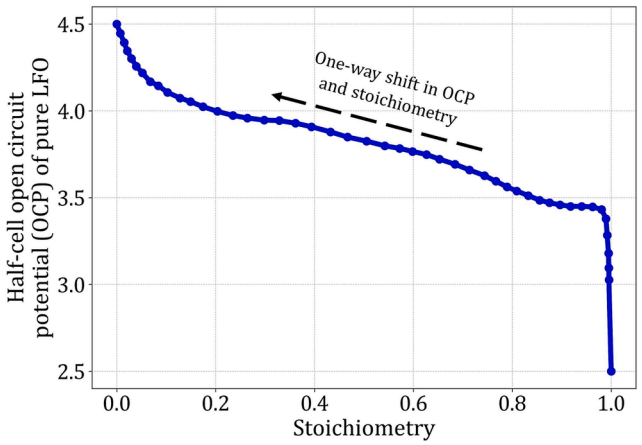


Figure 1. Half-cell OCP of a pure LFO material

Delithiation OCP of a pure LFO material with its stoichiometry.[10,16] The figure shows two voltage plateaus at OCP ~3.5 and ~4.0 V, corresponding to Equations 1 and 2.

We define the stoichiometry of fully lithiated LFO (i.e., Li_5FeO_4) as 1 with an OCP of 2.5 V and the stoichiometry of fully delithiated LFO (i.e., $LiFeO_2$) as 0 with an OCP of 4.5 V. As LFO releases its lithium irreversibly, its stoichiometry decreases monotonically from 1 to 0, and, correspondingly, its OCP increases from 2.5 to 4.5 V. When the composite PE potential drops below the OCP of LFO, no Faradaic reaction occurs on the LFO interface; i.e., lithium release from LFO stops until composite PE potential again increases above the LFO OCP. To release the lithium from LFO progressively and fully utilize it, LFO OCP may reach as high as 4.5 V, which can lead to electrolyte oxidation and the onset of Fe dissolution along with other unwanted parasitic reactions at the cathode-electrolyte interface and the gas evolution.[17–20] As is apparent from Equations 1 and 2, oxygen is co-released each time there is lithium release from the LFO, and overall, each mole of LFO released leads to the release of 1 mol of oxygen across the full LFO OCP range. While rarely discussed in the literature in the context of LFO, the presence of oxygen is known to contribute to different degradation mechanisms.[21–24] In this work, the oxygen-induced degradation and electrolyte oxidation are ignored, as it is assumed that most oxygen released from LFO is removed through cell degassing during the formation cycles.[25] We assume that any oxygen released later in the cell's life does not impact its degradation. Also, the study considers a carbonate-based electrolyte that has a stability window up to 4.3–4.5 V, and therefore, cathode degradation (e.g., Fe dissolution) along with other potential parasitic reactions at the cathode-electrolyte interface are neglected. While unlikely to be true, these assumptions may lead to quantitative errors in the model results; however, the qualitative observations are expected to remain unaffected, and the conclusions from the study are not expected to change. There is a distinct lack of experimental data that would enable a meaningful inclusion of these mechanisms in the model. It is worth noting that the moles

CellPress
OPEN ACCESS

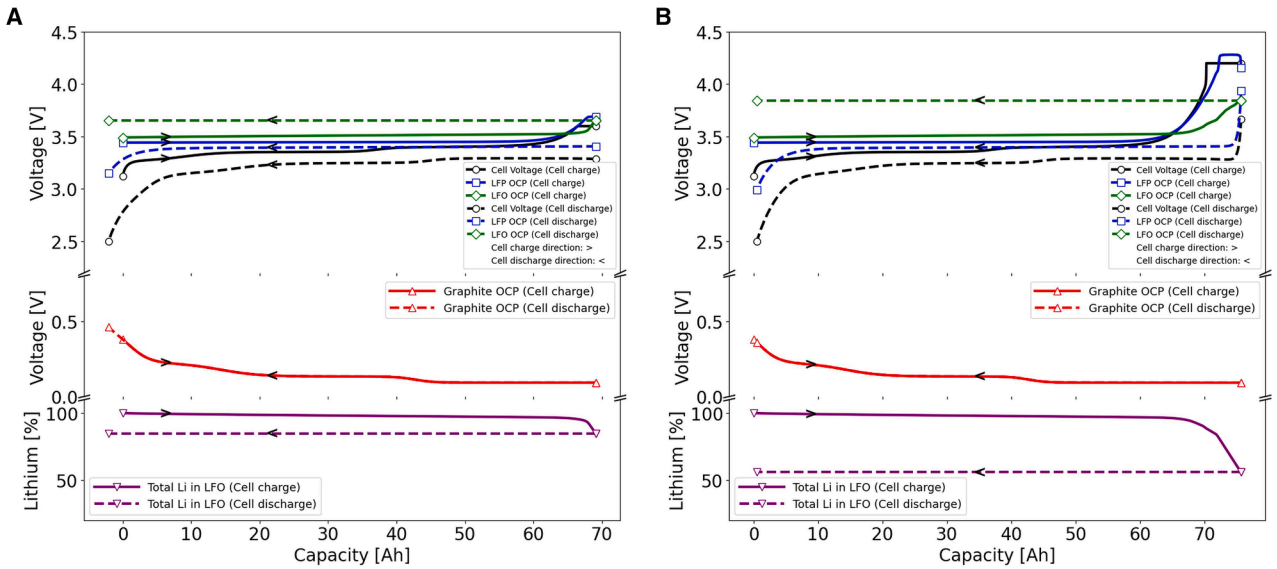


Figure 2. Relating the composite cell charging and discharging voltages to the lithium release from LFO and corresponding variations in the OCP of NE (graphite) and PE components (LFP and LFO)

Shown is the variation intrinsic to the model assumptions in the total lithium in LFO (in percentages, purple line, lower triangular markers), its bulk open circuit potential (OCP) (green lines, diamond markers), and the bulk OCP of graphite (red line, upper triangular markers) and LFP (blue line, square markers) during cell charging and discharging when the upper voltage cutoff for charging is set to (A) 3.6 V and (B) 4.2 V. The markers show the start and endpoints of the variations in the different variables during the charge and discharge process. The direction for cell charging (round markers, solid lines) and discharging (round markers, dashed lines) is represented by forward arrows and backward arrows, respectively. The high upper charging voltage cutoff (4.2 V in B) triggers the significant lithium release from LFO and permanently shifts the OCP of LFO to high OCP values. Cell discharging does not affect the lithium inventory in LFO and its OCP. The lower upper charging cutoff voltage (3.6 V in A) results in negligible lithium release from LFO.

of oxygen released depend upon the initial LFO moles and the LFO OCP. As 75% of the oxygen is released when the OCP of LFO reaches the second voltage plateau (~4.0 V), a lower LFO content and avoiding high cell charging voltages to avoid high OCPs of LFO would lead to significantly less oxygen release. Meanwhile, attempts are made to modify LFO by suitable coating layers and lattice engineering[26–28] to mitigate oxygen evolution and enhance performance. Oxygen release, its precise effect on cell degradation, and its mitigation are discussed in Note S3 in more detail. The gas evaluation, electrolyte stability, and interfacial degradation of the cathode are worthy of further experimental and modeling studies.

Correlating the composite LFP-LFO cell charging voltage to the LFO OCP and the associated lithium-oxygen release: Insights relative to a pure LFP cell

The first irreversible lithium release from LFO is triggered when the composite PE OCP exceeds the first plateau of LFO OCP of 3.5 V (Equation 1). Therefore, to use the Li stored in the LFO for a cell with a composite LFP-LFO cathode, the upper voltage cutoff during cell charging must be set to a value higher than 3.5 V. The operational voltage range for a pure LFP cathode-based cell is typically below 3.5 V, with the voltage plateau for normal operation located between 3.2 and 3.4 V, depending on state of charge and hysteresis. Even when accounting for overpotentials during operation, it is possible to keep the normal operating window for a pure LFP cathode-based cell below 3.5 V. As a result, the release of lithium and oxygen from the LFO component of a composite LFP-LFO cell can be fully controlled by carefully setting the upper cutoff voltage without affecting normal LFP cell operation. To demonstrate the expected behavior, a beginning of life (BoL) PyBaMM model was built (a detailed discussion of the PyBaMM model can be found in the first part of the next subsection and Note S1). The model was used to find the correlation of cell charging and discharging voltages to the lithium and oxygen release from LFO and its bulk average OCP and the variation in bulk average OCP of LFP and graphite. For this purpose, the two separate virtual experiments, each consisting of a single cycle of constant current (CC)-constant voltage (CV) charge followed by a CC discharge (both done at 0.1 C with a CV hold until the current reaches C/100), were simulated in the built PyBaMM model. An upper voltage cutoff for cell charging was set at 3.6 V (Figure 2A) and at 4.2 V (Figure 2B) for the first and second experiment, respectively. The lower discharge voltage cutoff for both experiments was kept at 2.5 V. Because the upper charging voltage cutoff of 3.6 V only slightly exceeds the first LFO OCP plateau of 3.5 V, this case releases only a small percentage (~10%) of total lithium moles in LFO (Figure 2A).

The released lithium moles shift the OCP of LFO slightly from ~3.5 to ~3.65 V. On the other hand, charging the cell to an upper cutoff of 4.2 V (Figure 2B) leads to the release of ~45% of the total lithium ion in LFO and a larger OCP shift (from ~3.5 to ~3.85 V). Also, it is expected that the second case would cause the release of significantly more oxygen than the first case, as the OCP here is close to the second plateau of LFO OCP

(Equation 2). This analysis indicates that the lithium and oxygen release from LFO can be fully controlled by setting the appropriate cutoff voltages during cell charging. Both figures also show that the cell discharging voltages do not impact the total lithium moles in LFO (flat dashed purple lines), which is the result of the informed assumption that cell discharging only lithiates the LFP component of the cathode; i.e., the LFO component of the cathode does not lithiate because of its irreversible sacrificial nature (Equations 1 and 2).

Exploring lithium and oxygen release from LFO during cell cycling using PyBaMM

To fulfill the goal of developing insights into how LFO can be employed and used in commercial LFP cells, we created a physics-based model in the open-source battery modeling environment, PyBaMM, which can simulate a large composite LFP-LFO cell. First, an isothermal BoL composite full-cell model was built, which was then modified to create a cell degradation model with SEI layer growth and lithium plating at the NE. A brief description of the model setup and assumptions is included in part 1 of the methods. More details on equations used in developing a composite BoL model and degradation (aging) model are given in Notes S1 and S2, respectively.

The final model was used to simulate lithium release from LFO and its consequences on cell degradation under 0.5 C charge and 0.5 C discharge. A reference performance test (RPT) was performed virtually every 25 charge-discharge aging cycles to emulate experimentally relevant protocols. Before each RPT, a controlled lithium release charging event was performed, and the oxygen was co-released each time there was lithium release from the LFO. During our baseline lithium release charging event, the cell was overcharged until the cell voltage reached 4.2 V, and then the cell was rested for 1 min. Although this represents an extreme lithium and oxygen release event, and it is possible to release them in a more controlled way by overcharging to lower voltages and/or for shorter times, this is similar to how LFO has been used and studied in most academic research to date.[9,10,12] Five lithium release control methods/cases were developed, using controlled charging events to create different patterns of lithium release from LFO. These methods were evaluated based on how their corresponding lithium and oxygen release patterns impacted cell life. As discussed before, each mole of lithium released from LFO theoretically releases an equal mole of oxygen; therefore, the oxygen release pattern is obtained by mirroring the lithium release behavior for various control methods/cases. This is briefly analyzed and compared in Figure S7. The potential effect of oxygen release on cell degradation is discussed in Note S3. Cases 1–4 were designed to investigate the impact of lithium release speed (fast or slow) and timing (early or late in cell cycle life) on cell life, while case 5, a non-conventional lithium release control method, was designed based on coulomb counting controlled charging (fixed capacity charging). As described previously, for each case, the simulation includes a break-in cycle and an initial RPT (both happen only once), followed by the set of 25 charge-discharge aging cycles, a controlled lithium release event (which is either a normal charging, an overcharging, or a coulomb-counted

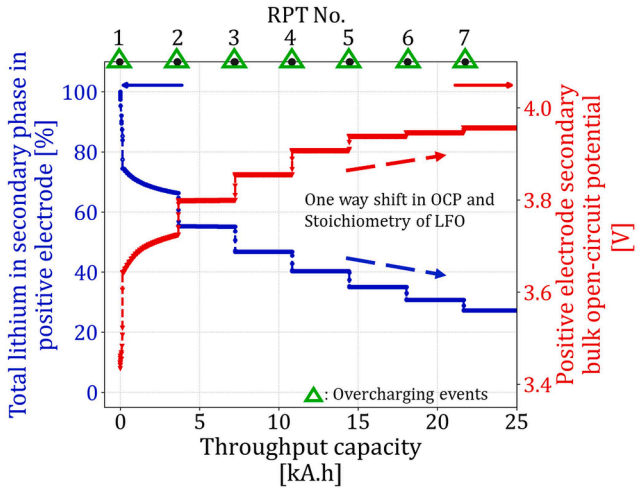


Figure 3. Lithium release from LFO with cycling and its effect on the OCP of LFO

Model prediction shows how lithium release affects the bulk OCP of LFO. As lithium is released from LFO, the percentage of lithium moles in LFO (total lithium in the secondary phase in PE [%], blue line, left *y* axis) drops with cycling, and that leads to increased bulk OCP (PE secondary bulk OCP [V], red line, right *y* axis). The change in bulk OCP and percentage of lithium (i.e., stoichiometry of LFO) is permanent and one way; this is as expected from experiments (shown in Figure 1). This model result is for a cell with 4% LFO fraction, cycled as per the protocol defined for case 1. The abrupt drop in lithium moles in LFO and the accompanying momentary spikes in its OCP are triggered by the overcharging event performed before each reference performance test (RPT) in case 1. For simplicity, only the first seven RPTs (175 aging cycles) and the aging cycles (175 aging cycles) completed between the first seven RPTs are shown. The data points correspond to the start of the discharge step in the aging cycles (refer to the virtual experiment in Figure 9).

controlled charging), and an RPT, all three repeated 80 times to achieve 2,000 charge/discharge aging cycles. Detailed information on setting up virtual experiments in PyBaMM and designing all five cases can be found in Figure 9 and Figure 10, respectively.

Figures 3 and 4 show model predictions for a commercial cell with 4% LFO active material volume fraction (extra added LFO volume fraction as a percentage of LFP active material volume fraction; Equation 11 in Table S1), subjected to controlled lithium release via an overcharging event before each RPT; i.e., case 1.

For simplicity, both figures display the performance during the first seven RPTs only (175 aging cycles) because nearly all LFO lithium is released in this time frame. As discussed earlier, each mole of LFO releases 4 moles of lithium; therefore, an active volume fraction of 4% is assumed to release sufficient lithium to compensate for ~16% of LLI. This level of LLI is typically observed over the entire first life of a cell (~80% state of health). Hence, 4% LFO, in principle, is sufficient to achieve zero degradation and was thus chosen in this study. This choice is also supported by announcements from CATL and Rimac Energy, which hinted toward 4%–5% LFO content in their cells. Additionally, a low LFO fraction ensures that less oxygen is released, avoiding oxygen-triggered degradation.

Figure 3 shows that, during the break-in cycle, first RPT and the first set of 25 normal charging-discharging aging

CellPress
OPEN ACCESS

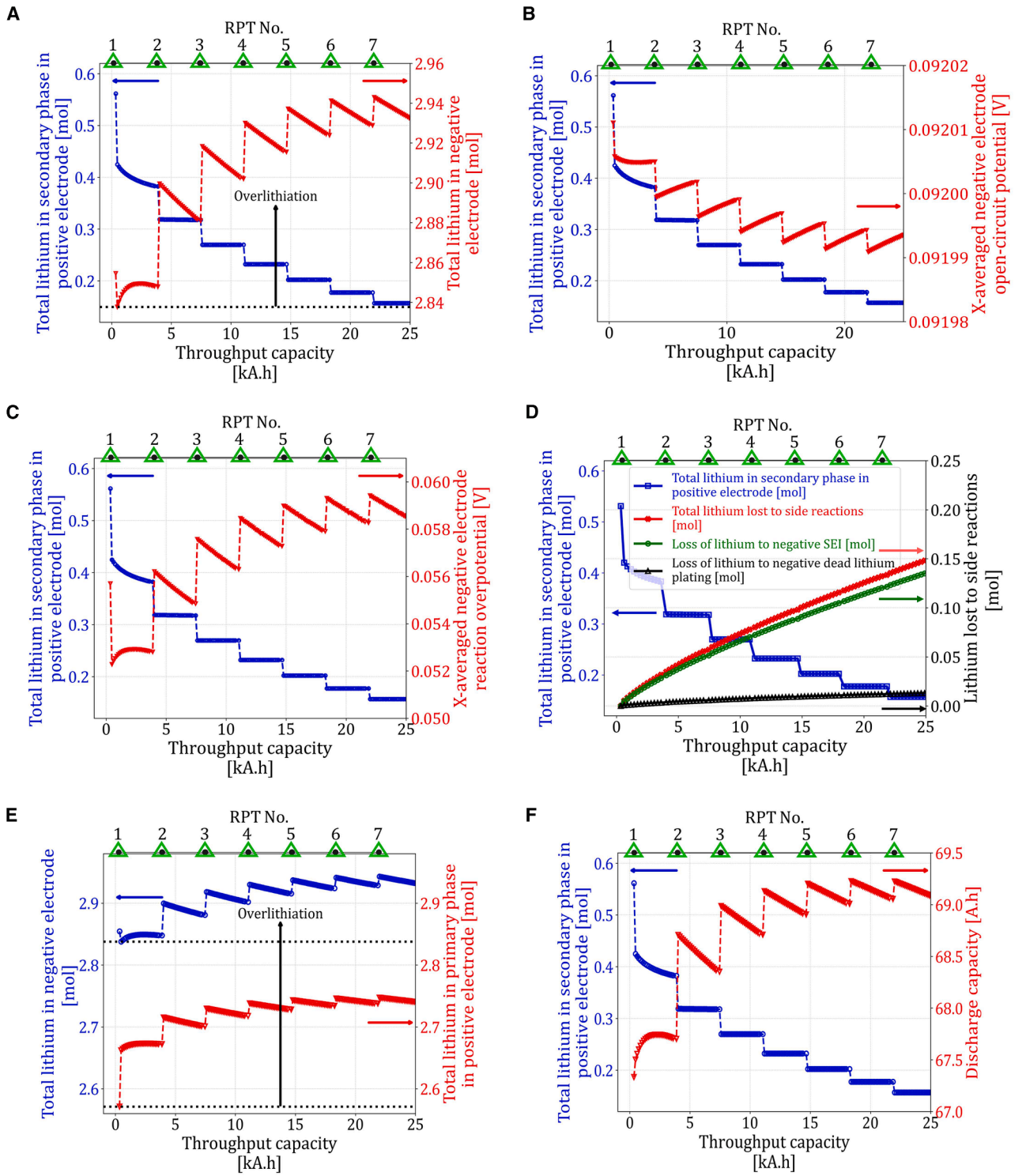


Figure 4. Lithium release from LFO and its impact on cell performance

(A) Total lithium in the secondary phase in PE (mol)(blue line, left *y* axis), and total lithium in NE (mol)(red line, right *y* axis) vs. throughput capacity (kAh). A dashed horizontal black line marks the balanced NE at the beginning of life (BoL).

(B) Total lithium in the secondary phase in PE (mol) (blue line, left *y* axis) and x-averaged NE OCP (V) (red line, right *y* axis) vs. throughput capacity (kAh).

(C) Total lithium in the secondary phase in PE (mol) (blue line, left *y* axis), and x-averaged NE reaction overpotential (V)(red line, right *y* axis) vs. throughput capacity (kAh).

(legend continued on next page)

cycles (before RPT 2), some lithium was released from the LFO (left *y* axis in Figure 3), as each of these normal charges had an upper voltage cutoff of 3.6 V. This voltage exceeds the first plateau of LFO OCP of 3.5 V (1), triggering irreversible lithium release from LFO, causing the stored lithium to drop from 100% to ~67%. The first overcharging event (just before RPT 2), with an upper voltage cutoff of 4.2 V, leads to a further release of ~12% lithium moles from LFO, decreasing the stored lithium percentage to ~55%. Overall, a significant amount of lithium was released (~45%) into the cell by the time the cell operation reached the end of the first overcharging event. For a cell with optimal balancing at the BoL, this release results in an already unbalanced cell. The effect of this imbalance on cell degradation, its capacity, and life is explored in the next subsection (Figure 4). The early and fast lithium release from LFO also increases its OCP significantly (right *y* axis in Figure 3), with the LFO OCP rising to ~3.8 V by the end of the first overcharge. During the next 25 normal charging-discharging aging cycles, no further lithium release occurs (stored lithium in LFO lithium kept at 55%), as the upper cutoff voltage limit for normal charging remains capped at 3.6 V, which is insufficient to overcome LFO OCP of 3.8 V (flat lines between RPT 2 and RPT 3 in Figure 3). The second overcharge event (just before RPT 3), with an upper voltage cutoff of 4.2 V, exceeds the LFO OCP of 3.8 V, triggering a further lithium release from LFO and dropping its storage percentage to ~47%. Note that only 8% of lithium is released in the second overcharging event (from 55% to 47%) compared to the 12% (from 67% to 55%) lithium release during the first event and decreases significantly in the subsequent overcharging events. This indicates that, as LFO depletes its lithium inventory, further lithium release from the LFO becomes increasingly difficult. This is because the LFO OCP eventually reaches close to the cell's upper voltage cutoff of 4.2 V, and then even higher overcharging cutoff voltage limits would be required to access the remaining lithium stored in the LFO.

Most previous academic research[10,12] has explored the use of lithium inventory as a sacrificial agent, either in a one-off event[10] (i.e., all lithium released during the first overcharge) or through the first few overcharges.[12] With the aim of explaining how LFO additives may be used optimally, we study a more controlled and gradual lithium release, the benefits of which are explained in the following subsections.

Consequences of lithium release from LFO on SEI growth, lithium plating, and cell usable capacity

When lithium is released from LFO, it can have both a positive and a negative impact on cell performance. In case 1, the lithium is released fast and early at a rate faster than lithium consumed by the side reactions. This disturbs the cell balancing as the electrodes are forced to host the extra unconsumed lithium inventory, leading to the over-lithiation of NE and primary phase in PE (i.e., LFP), as shown in Figures 4A and 4E. This causes the average OCP (particle surface OCP) of the NE to shift to lower potentials at the end of the charge, pushing it closer to zero (Figure 4B) and increasing the reaction overpotentials (Figure 4C). This accelerates the side reactions for SEI layer growth[15,29] and dead lithium plating,[15,30] leading to faster degradation and faster LLI. Therefore, if lithium from the LFO is released too fast, then it accelerates the precise problem it is there to mitigate. However, it is not all bad; the amount of lithium lost due to the accelerated side reactions does take time to equal the amount released and leads to a temporary higher discharge capacity (usable as well as cyclable lithium discharge capacity), their BoL values. As shown in Figure 4D at around 25 kAh throughput, ~0.15 moles have been consumed by side reactions, while ~0.4 moles were released from the LFO; the remaining 0.25 lithium moles are responsible for increased usable discharge capacity compared with its BoL value (Figure 4F).

From this analysis, it is clear that releasing too much lithium, although temporarily beneficial in proving a boost to the cell discharge capacity, eventually leads to accelerated side reactions (SEI and dead lithium plating) and, therefore, a potentially reduced cell lifetime. In the next sections, we show that the key to achieving longer lifetimes lies in the careful control of the lithium (and thus oxygen) release from LFO. The best control method may be the one that either delays the lithium release and avoids overlithiation from the start or the one that matches the lithium release rate from LFO with the lithium lost to side reactions without unbalancing the cell and accelerating the side reactions. This is explored in the next subsection.

Lithium release control methods and their effect on cell performance

With the help of case 1, we showed how fast and early lithium release from LFO can impact cell performance. We now investigate four additional patterns/cases (case 2 to case 5) of lithium

(D) Total lithium in the secondary phase in PE (mol) (blue line, left *y* axis), total lithium lost to side reactions (mol) (red line, right *y* axis), loss of lithium to negative SEI (mol) (green line, right *y* axis) and loss of lithium to negative dead lithium plating (mol) (black line, right *y* axis) vs. throughput capacity (kAh).

(E) Total lithium in NE (mol) (blue line, left y axis) and total lithium in primary phase in PE (mol) (red line, right *y* axis) vs. throughput capacity (kAh). Dashed horizontal black line marks the balanced NE and primary PE at BoL.

(F) Total lithium in the secondary phase in PE (mol) (blue line, left *y* axis) and discharge capacity (Ah) (red line, right *y* axis) vs. throughput capacity (kAh). For simplicity, the plot only shows the variation in the usable discharge capacity of the cell. The discharge capacities obtained from the discharge step in aging cycles are referred to as usable discharge capacities. The discharge capacities obtained from discharge RPTs are referred to as cyclable lithium discharge capacities. Though not shown in this plot, cyclable lithium discharge capacities are usually higher than the usable discharge capacities, as RPTs are done at lower C rates than aging cycles.

In all plots except in (E), the total lithium in the secondary phase in PE (mol) (i.e., total lithium moles in LFO) is shown on the left *y* axis (blue line). These model results are for a cell with 4% LFO fraction, cycled as per the protocol defined for case 1. The abrupt drop in total lithium moles in LFO and the accompanying abrupt changes in the values of variables on the right *y* axis are triggered by the overcharge event performed before each RPT in case 1. In (E), the spikes (i.e., the spike in the value of the variable plotted on the left *y* axis and the variable plotted on the right *y* axis) correspond to the overcharge event discussed above. For simplicity, only the aging cycles (175 aging cycles) completed between the first seven RPTs are shown. The data points correspond to the start of the discharge step (i.e., end of charge step) in the aging cycles (refer to the virtual experiment in Figure 9).

release in a cell with 4% LFO content and their impact on its performance. The cell performance was compared by studying how the discharge capacity and cell degradation indicators, such as LLI, SEI, lithium plating, and NE porosity, evolve with cell capacity throughput. For simplicity, only figures related to the comparison of case 1, case 4, and case 5 are shown here; for the comparison of case 1 with case 2 and case 3 and all five cases, see Figures S1 and S2).

As for case 1, case 2 to case 4 show that, whenever the overcharge events occur, the release of lithium from LFO happens rapidly (Figure 5A), leading to increased cyclable lithium discharge capacity (Figure 5B) as well as increased total lithium loss to the side reactions (increased SEI growth and dead lithium plating) (Figures 5C–5E). The formation of SEI and plating clogs the porosity of the NE in the model, leading to its decreasing trend (Figure 5F). Case 1 offers higher discharge capacities because of early and fast/frequent lithium release but significantly accelerates cell degradation and NE pore clogging. Case 2 delays the lithium release and, hence, can provide higher discharge capacities later in the cell life. Case 3, due to just four overcharge events, preserves most of the available lithium inventory from LFO, resulting in relatively slower cell degradation but also lower discharge capacity. In this case, the cell remains balanced due to less lithium released from LFO. Case 4 offers a better trade-off between degradation rates and discharge capacities due to the periodic nature of its lithium release. Periodic delays in lithium release provide enough time for side reactions to consume extra lithium from LFO. This helps in maintaining the cell closer to its balanced state despite the short imbalance caused every time an overcharge event triggers the fresh lithium release from LFO. As a result of insights gained from cases 1–4, case 5 was designed, in which the cell is overcharged until the cell charge (coulomb-counted charging) exactly matches its BoL cyclable lithium discharge capacity value (first RPT cycle discharge capacity) or the charging voltage reaches the maximum cutoff value of 4.2 V, whichever is earlier. This contrasts with the other cases, in which every overcharge event has a charge voltage cutoff limit of 4.2 V. Case 5 ensures that the released lithium moles from LFO are close to equal and, most importantly, do not overly compensate the lithium lost to the side reactions since the last overcharge/RPT. This more balanced and gradual release of lithium moles from LFO (Figure 5A) results in close to constant cyclable lithium discharge capacity (Figure 5B), moderate degradation rates, and reduced pore clogging (Figures 5D–5F). For all cases where lithium moles from LFO get depleted and/or are not enough to compensate for lithium loss due to side reactions, the sudden drop in discharge capacity is observed. This is because of the shift from overcharging/coulomb-counted charging to normal charging, where the charging is capped to the voltage cutoff limit of 3.6 V.

The maximum charging voltage during the controlled lithium release events in case 5 is variable, as the charging is controlled by fixed capacity; i.e., until the cell's charging capacity equals its BoL cyclable lithium discharge capacity. As a result, the average LFO OCP (particle surface OCP) increases gradually with cycling (Figure S3). Since the cell in this case operates below 4.2 V LFO OCP for most of the lithium release events, it is expected that the associated oxygen release would be gradual, potentially allowing cathode coating agents to effectively scavenge it. In real applications, charges are often done with a CV hold; if all five cases were to include one, case 5 would be expected to perform even better than case 1 and case 4 because of its lower operational LFO OCP. This is because holding the cell at high charging voltages (or high LFO OCP) is expected to accelerate oxygen evolution. For this reason, case 1 and case 4 would need careful consideration if implemented in real systems; case 5 has the most potential for real application.

These findings indicate that details of the exact control method adopted for lithium and oxygen release can significantly alter the performance of an LFO-enriched cell. Hence, based on the targeted operating conditions and cell performance requirements, LFO-aware control algorithms must be designed and implemented to tailor the timing and rate of lithium release.

Effect of LFO volume fraction on cell performance

In the previous section, case 5 is shown to have relatively better performance and the most potential in real applications compared to other cases at a 4% LFO fraction. Therefore, we now choose case 5 to explore the effect of 0.1%, 1%, and 10% LFO volume fractions on cell performance and compare it with the previously discussed case of 4% LFO. The case of 0.1% LFO is intentionally chosen, as the cell behavior in this case would be the closest representation of the pure LFP-Gr cell.

For the 0.1% and 1% LFO, the initial available lithium inventory is low (Figure 6A), and as the cell degrades, the lithium from LFO becomes depleted early, and, hence, the added benefit is short lived. For 0.1% LFO, all of the lithium in LFO is depleted at around 90 kAh (Figure 6B) throughput capacity, and, hence, the sudden drop in capacity is observed. For both the fractions, the total degradation rate due to side reactions (SEI and dead lithium plating) and NE porosity clogging is comparatively lower than for the 4% and 10% LFO fraction (Figures 6C and 6D). Because of the relatively small amount of lithium added by the LFO, the cell balancing remained relatively stable.

The 10% LFO cell contains significantly more lithium inventory to begin with, leading to a cyclable lithium discharge capacity that is considerably higher (Figures 6A and 6B) than for 0.1%, 1%, and 4% LFO cells. This benefit, however, is temporary; a steep drop in the discharge capacity is observed later in cell life (Figure 6B). Also, excessive availability of lithium inventory from LFO for longer periods keeps the cell in a highly unbalanced state (highly overlithiated NE) for longer, leading to accelerated side reactions (Figure 6C) and NE porosity clogging (Figure 6D). This leads to cell failure when NE gets clogged completely (zero porosity). The effect of 10% LFO fraction on cell performance for all five cases can be found in the Document S1 (Figures S4 and S5).

These findings reveal a clear trade-off between discharge capacity and long-term cell performance for a chosen LFO fraction. Additionally, a higher fraction of LFO would also lead to excess oxygen evolution, whose effect on degradation cannot be ignored. Hence, one must carefully choose the optimal volume fraction of LFO by looking at the desired cell performance over time.

Redesigning the cell to avoid cell unbalancing due to NE overlithiation

The model results in the previous sections revealed that, when the cell is perfectly balanced for BoL, even with moderate LFO

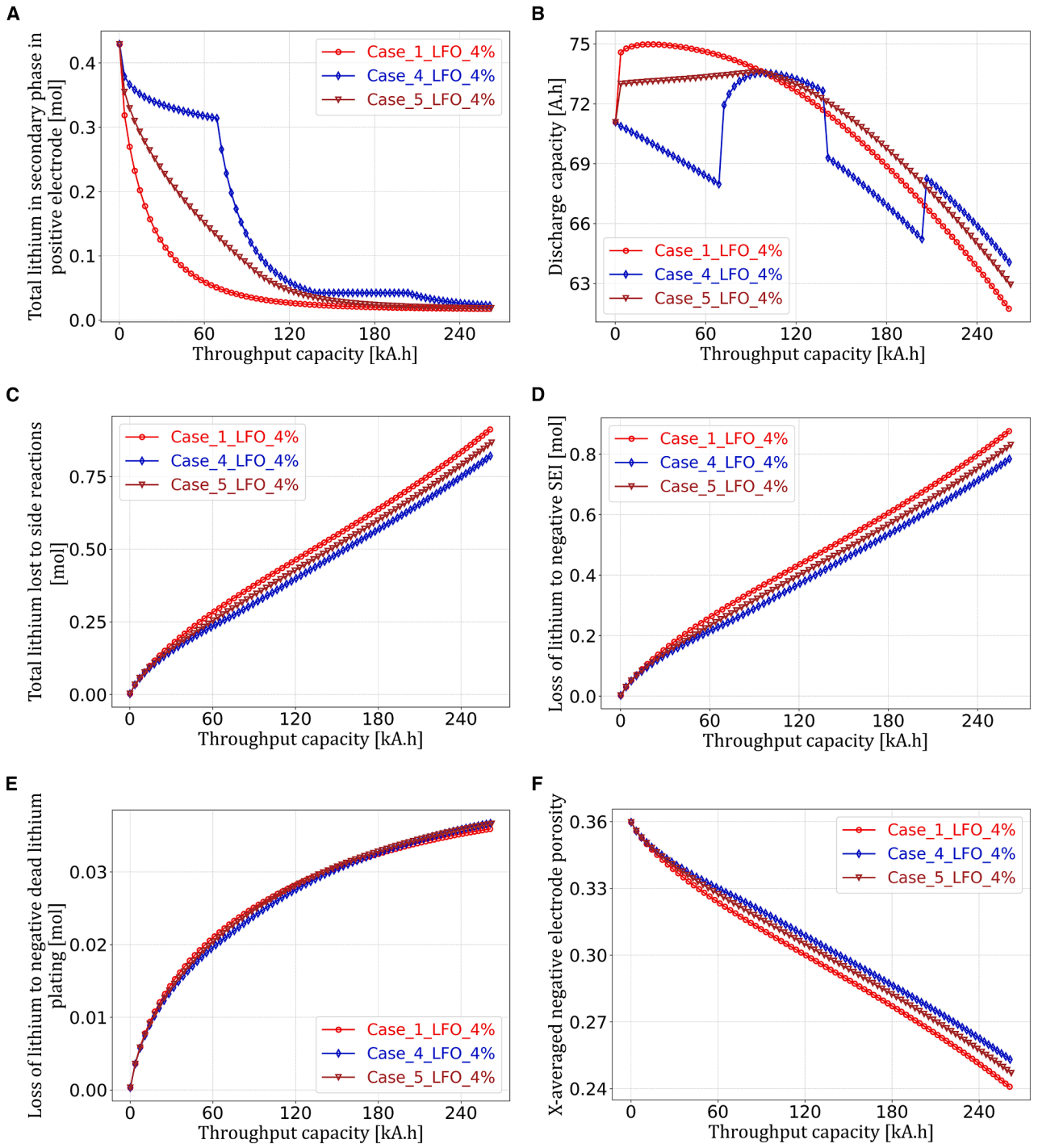


Figure 5. Comparison of cell performance for cases 1, 4, and 5 at 4% LFO fraction

Shown are (A) lithium release from the secondary phase (i.e., LFO), (B) cyclable lithium discharge capacity (RPT cycles discharge capacity), (C) total lithium lost to side reactions, (D) lithium lost to NE SEI, (E) lithium lost to NE dead lithium plating, and (F) average NE porosity (spatially averaged in the *x* direction) in an LFP-LFO composite cell for case 1 (red line, circle markers), case 4 (blue line, diamond markers), and case 5 (brown line, triangle markers).

content (e.g., 4% LFO), the lithium release from LFO overlithiates the electrodes, creating an unbalanced cell and accelerating degradation. We explored some of the possible control methods to manage cell overlithiation and degradation, but even the best control could not erase the negative effect of lithium release on cell balancing. For this reason, we conclude that a cell with an LFO additive must be balanced to accommodate the extra lithium to be released from LFO during controlled lithium release

CellPress
OPEN ACCESS

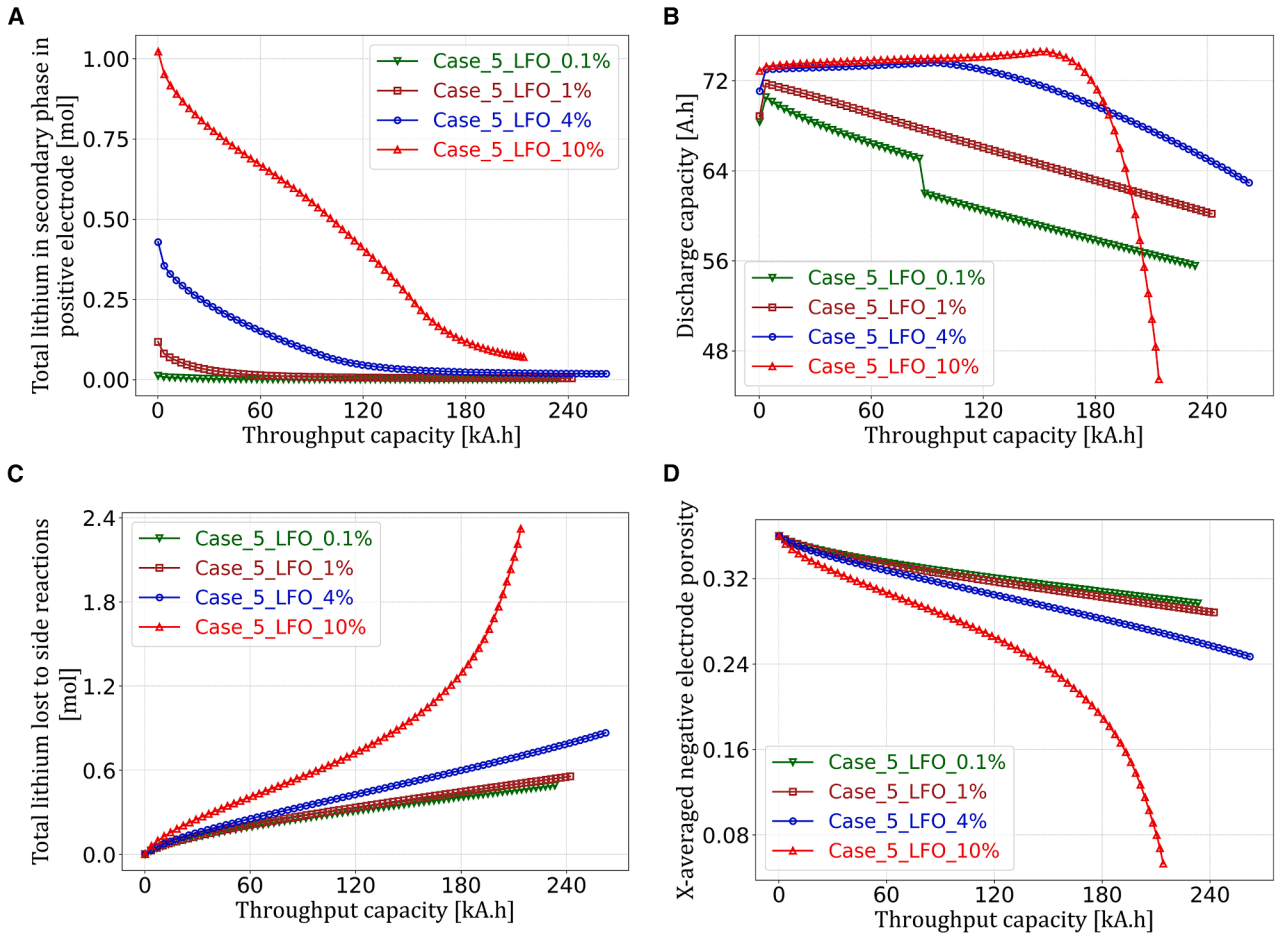


Figure 6. Comparison of cell performance for case 5 at 1%, 4%, and 5% LFO fraction

Shown are (A) lithium release from the secondary phase (i.e., LFO), (B) cyclable lithium discharge capacity (RPT cycles discharge capacity), (C) total lithium lost to side reaction (SEI + dead lithium plating), and (D) average NE porosity (spatially averaged in the *x* direction) in an LFP-LFO composite cell for 1% LFO (brown line with square markers), 4% LFO (blue line with circle markers), and 10% LFO (red line with triangle markers).

events rather than for BoL performance. Here, we propose a way to achieve such balancing by redesigning our composite LFP-LFO PyBaMM cell using a higher-capacity NE.

As an example, we increased the NE capacity by increasing the NE thickness so that the NP ratio increases from 1.1 (reference case) to 1.25, taken as the ratio of the NE capacity (graphite) to the primary phase of PE (LFP) capacity. The reference case is that of a BoL balanced cell, discussed in previous sections. While increasing the NE capacity, the other fundamental physical properties (maximum surface concentration, active material volume fraction, and electrode area) of the NE were kept unchanged. To compare the performance of the redesigned cell with that of the reference cell, the BoL performance of both was matched by adjusting the initial stoichiometries of NE and primary PE. To compare the long-term performance of the redesigned and reference cell, we chose case 1 as the lithium release control method because the frequent overcharges in case 1 were found to cause the most severe cell imbalance. Also, frequent overcharges, like in case 1, are expected, where the cell designers or process engineers may choose to intentionally perform frequent overcharge events (as in case 1) so that oxygen can be released and degassed early (for example, during early cell life after formation). Moreover, CATL also hinted at releasing lithium from LFO early in cell life. This makes case 1 a useful scenario for studying the benefits of cell redesign.

Figure 7 compares the case 1 performance for the reference case NP ratio of 1.1 and the redesigned NP ratio of 1.25 for 4% LFO content. A high cyclable lithium discharge capacity in case of a 1.25 NP ratio was maintained for a much longer cycle life than the 1.1 NP ratio (Figure 7A). This is due to less overlithiation and cell degradation rates leading to lower lithium loss to the side reactions (Figure 7B). The benefit of cell redesign on cell performance is expected to be more pronounced for a cell with a higher LFO fraction (e.g., 10%), as observed in Figure S6 in Document S1. Additionally, Figure S8 further highlights the benefit of the redesigned cell, even for the better-performing case 5, by comparing the cell performance for cells with NP ratios of 1.1 and 1.25 at 4% and 10% LFO fraction, respectively.

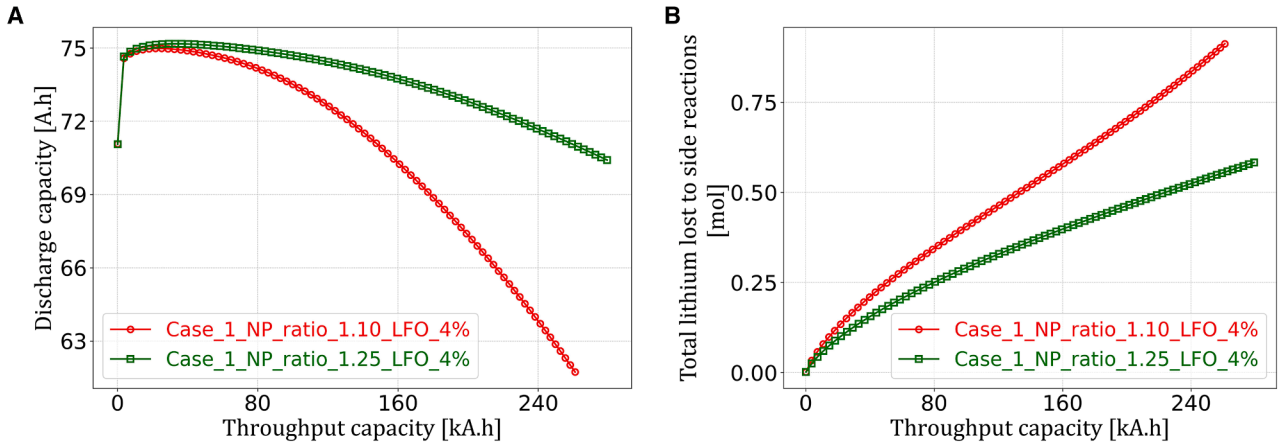


Figure 7. Comparison of cell performance when starting with perfect balance (NP ratio of 1.1) vs. starting with an imbalanced cell (NP ratio of 1.25) for case 1 at 4% LFO fraction

Shown are (A) cyclable lithium discharge capacity (RPT cycles discharge capacity) and (B) total lithium lost to side reaction (SEI + dead lithium plating) for an NP ratio of 1.1 (red line with round marker) and an NP ratio of 1.25 (green line with square marker). The NP ratio is referred to as the ratio of NE capacity (i.e., graphite capacity) to primary phase PE capacity (i.e., LFP capacity).

Hence, it is clear that the redesign of the cell away from the chosen base case NP ratio of 1.1 (the ratio in the typical reported intervals),[31–33] can benefit its longevity considerably. A larger NE overhang, however, would lead to lower cell energy density. A systematic optimization of the NP ratio is not performed in this work because the PyBaMM DFN framework does not capture the spatial effects associated with anode overhangs, which become increasingly important at higher NP ratios and can negatively impact overall cell performance.[34] The optimal NP ratio should be identified using advanced models capable of resolving spatial effects, and will be specific to the lithium release control strategy chosen and the targeted LFO fraction. This is beyond the scope of this work.

Taken together, these findings provide a comprehensive understanding of how lithium release control, LFO content, and cell design influence cell degradation and long-term cell performance.

We have modeled, for the first time, the effect of LFO additives on the long-term performance and degradation of LFP cells to retrieve the behavior of so-called zero-degradation lithium-ion batteries. A composite cathode (LFP-LFO) was developed, implemented in the open-source battery modeling environment PyBaMM, coupled with a graphite anode, and parametrized to simulate a large commercial composite LFP-LFO cell. The model included degradation because of SEI layer growth and lithium plating at the NE. This enabled us to study the effects of degradation, including capacity loss, cell unbalancing, and porosity clogging, on the life performance of the cell.

Different patterns of releasing the lithium from the LFO were explored to enhance capacity and to compensate for the effects of degradation. It was found that rapid release of excessive lithium could temporarily enhance cell capacity but led to intracell imbalances and increased degradation rates, resulting in reduced capacity in the long run. Gradual release of lithium to match and compensate for lithium lost due to degradation could maintain capacity for as long as LFO was not fully depleted of its lithium inventory. The direct consequences of oxygen evolution, associated with delithiation of LFO, were not modeled; this phenomenon is expected to affect lithium release strategies and needs to be studied further, both experimentally and in models. Various amounts of LFO, 0.1%, 1%, 4%, and 10% (by volume added LFO), were explored. 0.1% and 1% were too little to deliver a significant benefit, 4% was sufficient but required careful control strategies, and 10% was too high for a cell balanced for BoL and caused excessive degradation and rapid capacity loss. Finally, we explored the effect of rebalancing/redesigning the cell not just for BoL but to account for the excessive lithium that might be released from LFO later in the cell's life. This was found to have a large positive impact on cell capacity throughout its cycle life, enabling the primary phase of PE (i.e., LFP) to be fully utilized while maintaining a reasonable NE capacity excess/overhang to prevent accelerated degradation.

Overall, LFO can be a useful additive capable of delivering zero observable degradation for significant periods of time. To ensure its benefits, however, it requires careful optimization of the amount of LFO, initial balancing of the cell, charging strategy, controlled lithium release rate, and management of the oxygen released. The optimum combination of these factors is likely to be different for different applications and operating conditions. Multi-objective optimization problems are expensive to explore experimentally but ideal for a model-based approach. Therefore, the model presented in this paper should be of significant interest to anyone developing or considering the use of LFO-enriched lithium-ion battery cells. The model can also be easily adapted for other pre-lithiation or re-lithiation technologies being developed for any lithium-ion battery technology.

METHODS

PyBaMM model setup and model assumptions

The standard Doyle-Fuller-Newman (DFN)[35] model was set up in PyBaMM[15] using the model options listed in Figure 8. The details

CellPress
OPEN ACCESS

```
model_options = {
        SEI": ("interstitial-diffusion limited", "none"),
        "lithium plating": "partially reversible",
        "lithium plating porosity change": "true",
        "open-circuit potential": (("current sigmoid", "current sigmoid"), ("current sigmoid", "current sigmoid")),
        "SEI porosity change": "true",
        "intercalation kinetics": (("symmetric Butler-Volmer", "symmetric Butler-Volmer"), ("symmetric Butler-Volmer", "Tafel")),
        "particle phases": ("1", "2"),
    }
```

Figure 8. Snapshot of the PyBaMM code selecting the model options

about all the model options listed in Figure 8 can be found in the PyBaMM documentation.[36] A pure LFP graphite full cell BoL model was built and parameterized as in Prada et al.[37] and using estimated parameters so that it represented the performance characteristics of a typical large commercial pure LFP cell. The NE (i.e., graphite) and the primary phase of the PE (i.e., LFP) were balanced to achieve a base negative-to-positive ratio (NP ratio) of 1.1 (the NP ratio was defined as the ratio of NE [graphite] capacity to primary PE [LFP] capacity). The model equations and parameter values were then adapted to simulate a large composite LFP-LFO graphite full cell. This was done by including an additional set of equations accounting for different active material volume fractions of LFO and its electrochemical behavior. Since the NE was assumed to be graphite only, it was considered to have a single phase, whereas the composite PE had two phases: LFP as the primary phase and LFO as the secondary phase. Charge transfer kinetics for the NE single phase and PE primary phase (LFP) were modeled using Butler-Volmer kinetics. Tafel kinetics were chosen to model the LFO kinetics, as lithium release from LFO; i.e., its delithiation is a one-way irreversible process (Equations 1 and 2). Hysteresis in LFP was accounted for by considering the current sigmoid model in PyBaMM. To ensure simplicity and not to deviate from the primary goal of showing the proof of concept for designing a zero-degradation battery, the model was made to perform so that it was a close representative of actual LFP-LFO commercial cell behavior.

Once the BoL model was built and its performance was checked, the model was modified to create a full-cell degradation model. Only NE degradation is considered in this work. The degradation mechanisms, such as SEI formation, partially reversible lithium plating, and the resulting porosity clogging at the NE, were added to the PyBaMM model using the options listed in Figure 8. The SEI model considered in this study is adopted from Single et al.[38] and von Kolzenberg et al.[39] The partially reversible lithium plating model is unchanged from O'Kane et al.[30] Any degradation on the primary phase of PE (LFP) (i.e., due to its overdischarge/charge, which would have different magnitudes when different upper voltages cutoffs are chosen for LFO use) is not considered in this work.

The supplemental information contains the detailed discussion about the built PyBaMM model. BoL model equations are as listed in Table S1, and the degradation model equations are listed in Table S2. A detailed discussion of these equations can be found in Notes S1 and S2. The input parameters used in the BoL model are summarized in Tables S3 and S4. The parameter values for developing the degradation model are mentioned in Table S5. Descriptions of model variables, constants, their meaning, and symbols are summarized in Table S6.

As the work specifically focuses on the electrochemical effects of LFO additives in a commercial cell, an isothermal model was considered to intentionally omit the influence of temperature evolution, thermal gradients, and inhomogeneities on cell behavior. As the work was primarily aimed at demonstrating and explaining the science behind employing LFO by building a cell model that closely mimics the characteristics of real-life commercial LFP-LFO composite cells, the work intentionally omits the influence of temperature evolution, thermal gradients, and inhomogeneities on cell degradation. Additionally, the maximum charge discharge rates in the modeled were up to 0.5 C, which were assumed sufficiently low to ignore the thermal effect and the influence of thermally sensitive parameters on LFP-LFO cells. However, to consider the fast-charging scenarios for practical application and show the influence of higher charging rates during aging cycles on cell performance, we simulated two example cases by considering aggressive charging (1 C) during aging cycles. The results are shown in Figures S9 and S10, while Note S4 highlights the main observations.

Also, the work does not focus on experimental validation and performing a sensitivity analysis on various BoL and degradation-related parameters (information on BoL and degradation-related parameters can be found in Note S1). However, the modeling framework developed here is intended to guide, inform, and motivate future experimental investigations to validate and extend the findings reported in this paper. The modeling framework is also intended to act as a tool for exploration of novel chemistries like LFP-LFO and guide future researchers, control engineers, and cell designers by highlighting the trade-offs that are expected when creating and using chemistries like LFP-LFO batteries.

Setting up a virtual experiment in PyBaMM

The virtual experiments were designed in PyBaMM to simulate the long-term aging of a composite LFP-LFO full cell (Figure 9). The virtual experiment performs a break-in cycle, followed by a baseline RPT and then multiple repetitions of aging cycles, interspersed with characterization RPTs.

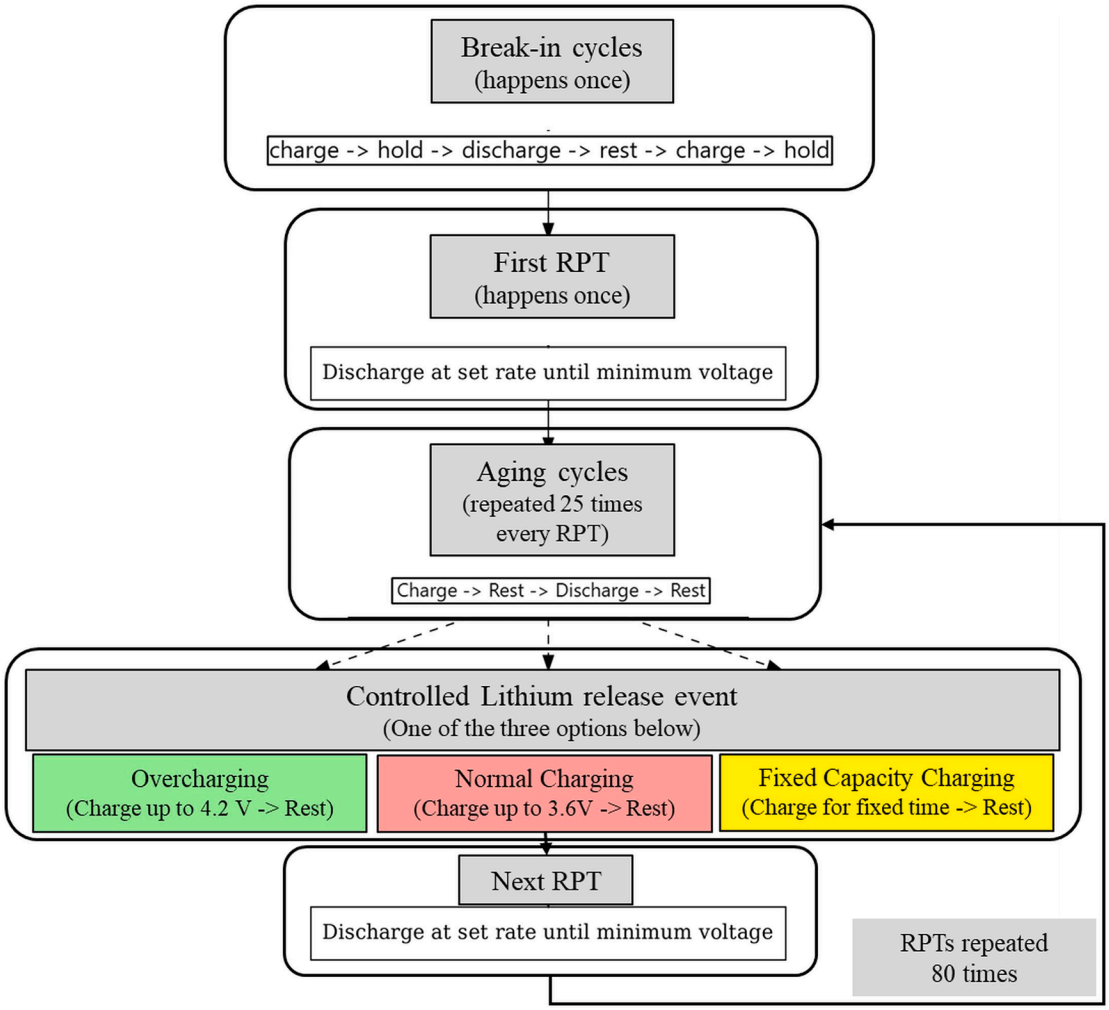


Figure 9. Snapshot of the virtual experiment considered in the PyBaMM model

The test starts with a breaking cycle that involves CC-CV charging (CC charge to upper voltage cutoff and CV hold till C/100), followed by CC discharge to a lower voltage cutoff and 1 h rest, and then CC-CV charging again. After that, the first RPT (RPT 1) was done with CC discharge to a lower voltage cut-off to measure BoL discharge capacity, and then the aging cycles were performed. Aging cycles consist of a set of 25 cycles of CC charge to upper voltage cutoff-rest (1 min)-CC discharge to lower voltage cut-off-rest (1 min) steps. This set of 25 aging cycles is followed by one controlled lithium release charging event; i.e., CC charge-rest (1 min) and an RPT. Depending upon the lithium release control pattern/case adopted (a discussion on cases can be found below), the controlled lithium release charge event could either be a normal charge, an overcharge (higher voltage cutoff), or capacity-controlled/coulomb-counted charging (fixed capacity charging). The set of 25 aging cycles, one controlled lithium release charging event, and a characterization RPT is then repeated 80 times to achieve 2,000 aging cycles. The discharge capacity obtained from discharges done during aging cycles was denoted as usable discharge capacity (or aging cycle discharge capacity), whereas discharge capacity obtained from RPT 1 and the 80 other RPTs is collectively referred to as cyclable lithium discharge capacity (or RPT cycle discharge capacity).

The charge and discharge rates considered for aging cycles and breaking cycles were 0.5 C, whereas the discharge rate for characterization RPTs was 0.2 C. For normal charging, the lower and upper cutoff voltage limits were 2.5 and 3.6 V, respectively. For overcharging, the voltage limits considered were 2.5 and 4.2 V, respectively. The upper limit of 4.2 V for overcharging was chosen as a commonly acceptable and practical limit in Li-ion cell operations. First, the limit allows us to be practical within the carbonate-based electrolyte stability window (<4.3 to −4.5 V), minimizing electrolyte oxidation, parasitic reactions at electrode-electrolyte interfaces, and gas evolution, which is currently not modeled in our work and could form part of future studies. Second, the 4.2 V voltage is sufficient to enable substantial lithium release from LFO by accessing the second voltage plateau of LFO, allowing for its better utilization. Last, the stable electrolyte, along with lower operating temperature, is also

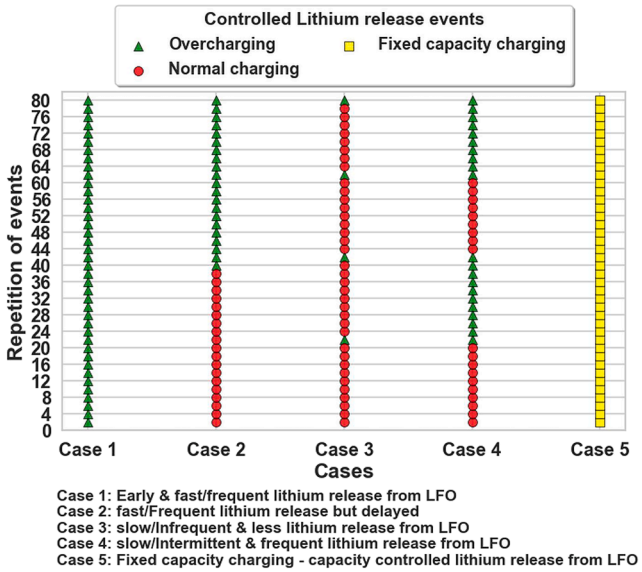


Figure 10. Different patterns/cases of lithium release events and their repetition/frequency

The figure shows the number of lithium release-controlled charging events just before characterization RPTs. Cases represent the different patterns of lithium release events. The green triangles represent an overcharging event, which is done just before its respective characterization RPT (RPT number on the *y* axis). The red dots represent a normal charging event done before the respective characterization RPT. The yellow squares represent a coulomb-counted (fixed-capacity) charging event, which is done just before its respective characterization RPT.

especially helpful in minimizing the cathode degradation pathways, such as Fe dissolution[19,20] at the LFP surface; hence, the choice of 4.2 V voltage cutoff provides a reasonable trade-off within the scope of this study.

Setting up lithium release patterns (cases) in PyBaMM

We designed five methods for lithium release, also called cases (Figure 10). These cases are designed to control the speed (fast or slow) and timing (early or later part of cell life) of lithium release from LFO.

Case 1 represents the early, fast, and frequent lithium release from LFO, in which overcharges are done before every RPT, thus totaling 80 overcharges. Case 2 illustrates fast and frequent lithium release starting later in the cell life, after cell throughput capacity becomes equivalent to 1,000 aging cycles. Here, overcharge is done starting from the 40th RPT (i.e., delayed lithium release from LFO) and repeats regularly, before each RPT between the 41st and 80th, thus totaling 40 overcharges.

Case 3 represents slow and infrequent lithium release, in which an overcharge is done regularly, before the 20th, 40th, 60th, and 80th RPTs, thus totaling only 4 overcharges. Case 4 represents the case of fast and frequent but periodic lithium release, in which overcharges are done continuously between the 20th to 40th RPT and then the 60th to 80th RPT, with a total of 40 overcharges. Case 5 performs coulomb-counted controlled charging (i.e., fixed-capacity charging), where the cell continues to charge until it achieves its BoL cyclable (RPT cycle) discharge capacity or hits the charging voltage upper cut-off safety limit of 4.2 V. This represents the case where we are indirectly calibrating lithium release to match the lithium lost to side reactions and, hence, avoid overlithiation of the NE.

RESOURCE AVAILABILITY

Lead contact

Requests for further information and resources should be directed to and will be fulfilled by the lead contact, Gregory James Offer (gregory.offer@imperial.ac.uk).

Materials availability

This study did not generate new, unique reagents.

Data and code availability

- The source raw data used for creating the plots in the manuscript are provided at Zenodo[40] and are publicly available as of the date of publication.
- All original code is deposited at the repository (https://github.com/srawat77/Codes-for-LFP-LFO-Composite-Paper.git) and is publicly available at Zenodo[40] as of the date of publication.
- Any additional information required to reanalyze the data reported in this paper is available from the lead contact upon request.

ACKNOWLEDGMENTS

This work was supported by the Faraday Institution (grant no. FIRG084).

AUTHOR CONTRIBUTIONS

S.K.R., conceptualization, validation, software, formal analysis, visualization, and writing – original draft; M.M., conceptualization, investigation, writing – review and editing, and primary supervision; G.J.O., conceptualization, writing – review and editing, secondary supervision, funding acquisition, and project administration; R.L., discussion; S.E.J.O., discussion.

DECLARATION OF INTERESTS

The authors declare no competing interests.

SUPPLEMENTAL INFORMATION

Supplemental information can be found online at https://doi.org/10.1016/j.xcrp.2026.103279.

Received: August 27, 2025
Revised: January 30, 2026
Accepted: April 6, 2026
Published: April 30, 2026

REFERENCES

1. Birkl, C.R., Roberts, M.R., McTurk, E., Bruce, P.G., and Howey, D.A. (2017). Degradation diagnostics for lithium ion cells. J. Power Sources *341*, 373–386. https://doi.org/10.1016/j.jpowsour.2016.12.011.
2. Edge, J.S., O'Kane, S., Prosser, R., Kirkaldy, N.D., Patel, A.N., Hales, A., Ghosh, A., Ai, W., Chen, J., Yang, J., et al. (2021). Lithium ion battery degradation: what you need to know. Phys. Chem. Chem. Phys. *23*, 8200–8221. https://doi.org/10.1039/d1cp00359c.
3. Peled, E., and Menkin, S. (2017). Review—SEI: Past, Present and Future. J. Electrochem. Soc. *164*, A1703–A1719. https://doi.org/10.1149/2.1441707jes.
4. Goodenough, J.B., and Kim, Y. (2009). Challenges for Rechargeable Li Batteries. Chem. Mater. *22*, 587–603. https://doi.org/10.1021/cm901452z.

5. Keil, P., Schuster, S.F., Wilhelm, J., Travi, J., Hauser, A., Karl, R.C., and Jossen, A. (2016). Calendar Aging of Lithium-Ion Batteries. J. Electrochem. Soc. *163*, A1872–A1880. https://doi.org/10.1149/2.0411609jes.

6. Bischof, K., Flügel, M., Hölzle, M., Wohlfahrt-Mehrens, M., and Waldmann, T. (2024). Aging Mechanism For Calendar Aging of Li-Ion Cells With Si/Graphite Anodes. J. Electrochem. Soc. *171*, 010510. https://doi.org/10.1149/1945-7111/ad1b7c.

7. Vetter, J.N.,P., Wagner, M.R., Veit, C., Möller, K.C., Besenhard, J.O., Winter, M., Wohlfahrt-Mehrens, M., Vogler, C., and Hammouche, A. (2005). Ageing mechanisms in lithium-ion batteries. J. Power Sources *147*, 269. https://doi.org/10.1016/j.jpowsour.2005.01.006.

8. Liu, Q., Du, C., Shen, B., Zuo, P., Cheng, X., Ma, Y., Yin, G., and Gao, Y. (2016). Understanding undesirable anode lithium plating issues in lithium-ion batteries. RSC Adv. *6*, 88683–88700. https://doi.org/10.1039/c6ra19482f.

9. Johnson, C.S., Kang, S.H., Vaughey, J.T., Pol, S.V., Balasubramanian, M., and Thackeray, M.M. (2010). Li2O Removal from Li5FeO4: A Cathode Precursor for Lithium-Ion Batteries. Chem. Mater. *22*, 1263–1270. https://doi.org/10.1021/cm902713m.

10. Liu, X., Liu, J., Peng, J., Cao, S., Hu, H., Chen, J., Lei, Y., Tang, Y., and Wang, X. (2024). Addressing the initial lithium loss of lithium ion batteries by introducing pre-lithiation reagent Li5FeO4/C in the cathode side. Electrochim. Acta *481*, 143918. https://doi.org/10.1016/j.electacta.2024.143918.

11. Dose, W.M., Maroni, V.A., Piernas-Muñoz, M.J., Trask, S.E., Bloom, I., and Johnson, C.S. (2018). Assessment of Li-Inventory in Cycled Si-Graphite Anodes Using LiFePO4as a Diagnostic Cathode. J. Electrochem. Soc. *165*, A2389–A2396. https://doi.org/10.1149/2.1271810jes.

12. Su, X., Lin, C., Wang, X., Maroni, V.A., Ren, Y., Johnson, C.S., and Lu, W. (2016). A new strategy to mitigate the initial capacity loss of lithium ion batteries. J. Power Sources *324*, 150–157. https://doi.org/10.1016/j.jpowsour.2016.05.063.

13. Pathirana, T. (2024). CATL's SECRET to "Zero" Degradation Batteries: Unveiling the Potential of LFO Cathode Additives. https://www.linkedin.com/pulse/catls-secret-zero-degradation-batteries-unveiling-lfo-pathirana-yfsuc/.

14. Murray, C.; Energy Storage News (Europe) (2024). https://www.energy-storage.news/catl-unveils-five-year-zero-degradation-bess-with-6-25mwh-per-container/.

15. Sulzer, V., Marquis, S.G., Timms, R., Robinson, M., and Chapman, S.J. (2021). Python Battery Mathematical Modelling (PyBaMM). J. Open Res. Softw. *9*, 14. https://doi.org/10.5334/jors.309.

16. Sepideh, A. (2017). *Lithium-Ion battery SOC Estimation* Doctor of Philosophy Thesis (University of Waterloo).

17. Xu, K. (2014). Electrolytes and interphases in Li-ion batteries and beyond. Chem. Rev. *114*, 11503–11618. https://doi.org/10.1021/cr500003w.

18. Li, W., Song, B., and Manthiram, A. (2017). High-voltage positive electrode materials for lithium-ion batteries. Chem. Soc. Rev. *46*, 3006–3059. https://doi.org/10.1039/c6cs00875e.

19. Simolka, M., Heger, J.F., Kaess, H., Biswas, I., and Friedrich, K.A. (2020). Influence of cycling profile, depth of discharge and temperature on commercial LFP/C cell ageing: post-mortem material analysis of structure, morphology and chemical composition. J. Appl. Electrochem. *50*, 1101–1117. https://doi.org/10.1007/s10800-020-01465-6.

20. Cai, J., Li, Y., Xu, S., Li, Y., Wang, Z., Liu, J., Yang, S., and Yan, X. (2025). A review on the insights into redox-based regeneration strategies for LiFePO4 batteries. Nanoscale *17*, 12048–12064. https://doi.org/10.1039/d4nr04671d.

21. Leanza, D., Mirolo, M., Vaz, C.A.F., Novák, P., and El Kazzi, M. (2019). Surface Degradation and Chemical Electrolyte Oxidation Induced by the Oxygen Released from Layered Oxide Cathodes in Li−Ion Batteries. Batter. Supercaps *2*, 482–492. https://doi.org/10.1002/batt.201800126.

22. Kaufman, L.A., and McCloskey, B.D. (2021). Surface Lithium Carbonate Influences Electrolyte Degradation via Reactive Oxygen Attack in Lithium-Excess Cathode Materials. Chem. Mater. *33*, 4170–4176. https://doi.org/10.1021/acs.chemmater.1c00935.

23. Adebanjo, I.T., Eko, J., Agbeyegbe, A.G., Yuk, S.F., Cowart, S.V., Nagelli, E.A., Burpo, F.J., Allen, J.L., Tran, D.T., Bhattarai, N., et al. (2025). A comprehensive review of lithium-ion battery components degradation and operational considerations: a safety perspective. Energy Adv. *4*, 820–877. https://doi.org/10.1039/d5ya00065c.

24. Chu, Y., Mu, Y., Zou, L., Wu, F., Yang, L., Feng, Y., and Zeng, L. (2024). Oxygen Release in Ni-Rich Layered Cathode for Lithium-Ion Batteries: Mechanisms and Mitigating Strategies. Chemelectrochem *11*, e202300653. https://doi.org/10.1002/celc.202300653.

25. Schomburg, F., Heidrich, B., Wennemar, S., Drees, R., Roth, T., Kurrat, M., Heimes, H., Jossen, A., Winter, M., Cheong, J.Y., and Röder, F. (2024). Lithium-ion battery cell formation: status and future directions towards a knowledge-based process design. Energy Environ. Sci. *17*, 2686–2733. https://doi.org/10.1039/d3ee03559j.

26. Zhu, B., Wen, N., Wang, J., Wang, Q., Zheng, J., and Zhang, Z. (2024). Defect engineering of air-stable Li(5)FeO(4) towards an ultra-high capacity cathode prelithiation additive. Chem. Sci. *15*, 12879–12888. https://doi.org/10.1039/d4sc03052d.

27. Kobayashi, H., Nakamura, Y., Yokoyama, Y., Honma, I., and Nakayama, M. (2024). Toward Cost-Effective High-Energy Lithium-Ion Battery Cathodes: Covalent Bond Formation Empowers Solid-State Oxygen Redox in Antifluorite-Type Lithium-Rich Iron Oxide. ACS Mater. Lett. *6*, 2072–2076. https://doi.org/10.1021/acsmaterialslett.4c00268.

28. Zhu, Y., Xu, R., Zheng, Y., Chen, Y., Yin, J., Xue, J., Zhang, B., Li, L., Zeng, G., Luo, H., et al. (2025). Unravelling the Oxygen Evolution Mechanism of Lithium-Rich Antifluorite Prelithiation Agent Based on Anionic Oxidation. Angew. Chem. Int. Ed. Engl. *64*, e202502126. https://doi.org/10.1002/anie.202502126.

29. Reniers, J.M., Mulder, G., and Howey, D.A. (2019). Review and Performance Comparison of Mechanical-Chemical Degradation Models for Lithium-Ion Batteries. J. Electrochem. Soc. *166*, A3189–A3200. https://doi.org/10.1149/2.0281914jes.

30. O'Kane, S.E.J., Ai, W., Madabattula, G., Alonso-Alvarez, D., Timms, R., Sulzer, V., Edge, J.S., Wu, B., Offer, G.J., and Marinescu, M. (2022). Lithium-ion battery degradation: how to model it. Phys. Chem. Chem. Phys. *24*, 7909–7922. https://doi.org/10.1039/d2cp00417h.

31. Zheng, H., Li, J., Song, X., Liu, G., and Battaglia, V.S. (2012). A comprehensive understanding of electrode thickness effects on the electrochemical performances of Li-ion battery cathodes. Electrochim. Acta *71*, 258–265. https://doi.org/10.1016/j.electacta.2012.03.161.

32. Abe, Y., and Kumagai, S. (2018). Effect of negative/positive capacity ratio on the rate and cycling performances of LiFePO4/graphite lithium-ion batteries. J. Energy Storage *19*, 96–102. https://doi.org/10.1016/j.est.2018.07.012.

33. Teng, J., Tang, X., Tang, M., Wu, Q., and Li, J. (2022). Failure mechanism and voltage regulation strategy of low N/P ratio lithium iron phosphate battery. J. Energy Storage *51*, 104588. https://doi.org/10.1016/j.est.2022.104588.

34. Kim, C.-S., Jeong, K.M., Kim, K., and Yi, C.-W. (2015). Effects of Capacity Ratios between Anode and Cathode on Electrochemical Properties for Lithium Polymer Batteries. Electrochim. Acta *155*, 431–436. https://doi.org/10.1016/j.electacta.2014.12.005.

35. Doyle, M., Fuller, T.F., and Newman, J. (1993). Modeling of Galvanostatic Charge and Discharge of the Lithium/Polymer/Insertion Cell. J. Electrochem. Soc. *140*, 1526–1533. https://doi.org/10.1149/1.2221597.

36. PyBaMM (2024). PyBaMM documentation. https://docs.pybamm.org/en/stable/.

37. Prada, E., Di Domenico, D., Creff, Y., Bernard, J., Sauvant-Moynot, V., and Huet, F. (2013). A Simplified Electrochemical and Thermal Aging Model of LiFePO4-Graphite Li-ion Batteries: Power and Capacity Fade Simulations. J. Electrochem. Soc. *160*, A616–A628. https://doi.org/10.1149/2.053304jes.

38. Single, F., Latz, A., and Horstmann, B. (2018). Identifying the Mechanism of Continued Growth of the Solid-Electrolyte Interphase. ChemSusChem *11*, 1950–1955. https://doi.org/10.1002/cssc.201800077.

39. von Kolzenberg, L., Latz, A., and Horstmann, B. (2020). Solid-Electrolyte Interphase During Battery Cycling: Theory of Growth Regimes. ChemSusChem *13*, 3901–3910. https://doi.org/10.1002/cssc.202000867.

40. Rawat, S. K. Raw Simulation Data from PyBaMM Modeling of Composite (LFP+LFO) Cathode and Graphite Anode in a Large-Format Lithium-Ion Cell; Data Supporting the Paper: How to Design a Zero-Degradation Battery: Compensating for Loss of Lithium Inventory in LFP Cells with LFO Additives. doi:https://doi.org/10.5281/zenodo.16583787 (2025).